

We are IntechOpen, the world's leading publisher of Open Access books Built by scientists, for scientists

6,900

Open access books available

186,000

International authors and editors

200M

Downloads

Our authors are among the

154

Countries delivered to

TOP 1%

most cited scientists

12.2%

Contributors from top 500 universities



WEB OF SCIENCE™

Selection of our books indexed in the Book Citation Index
in Web of Science™ Core Collection (BKCI)

Interested in publishing with us?
Contact book.department@intechopen.com

Numbers displayed above are based on latest data collected.
For more information visit www.intechopen.com



Tsunami Propagation Models Based on First Principles

A. Tan, A.K. Chilvery, M. Dokhanian and S.H. Crutcher

Additional information is available at the end of the chapter

<http://dx.doi.org/10.5772/50508>

1. Introduction

Tsunamis are ocean waves generated by the displacement of a large volume of water due to earthquakes, volcanic eruptions, landslides or other causes above or below the ocean floor (e.g., Karling, 2005; Parker, 2012). The great Indian Ocean tsunami of December 2004 will be remembered for its ferocity, devastation and unprecedented loss of life for a long time (Stewart, 2005; The Indian Ocean Tsunami, 2011). It is also the same tsunami which has galvanized the international community to set up warning systems and undertake preventive measures against the onslaught of future tsunamis in the vulnerable regions around the globe. A surge of scientific studies on all aspects of the tsunami is in evidence in the literature. And a volume entitled *“The Tsunami Threat – Research and Technology”* (Mörner ed., 2011) has been brought out. The current volume entitled *“Tsunami”* (Lopez, ed., 2012) is a sequel to the above in a continued effort to promote understanding and predicting future tsunamis and warning the populace in the potentially vulnerable areas.

There are three distinct stages of a tsunami event: (1) Generation; (2) Propagation; and (3) Inundation/landfall (cf. Cecioni & Belloti, 2011). The generation stage is the most complex and most difficult to analyze, since each tsunami is different and no single mechanism can account for all tsunamis. The inundation stage is also different for different areas affected, and again, no single scenario can describe all affected areas. The propagation stage covers the most extensive area, and is the only one that can be attacked by simple theory and analysis, even though detailed numerical models are found in the literature (see, for example, Imteaz, et al., 2011, and the references therein). These models consist of solving hydrodynamic equations with suitable boundary conditions that necessarily involve tedious numerical integrations. Such models, unfortunately, fall within the realm of the specialists, and are, by and large, outside the reach of the broader audience.

This chapter takes an alternative approach to the study of tsunami propagation in the open ocean. It commences with the theory of water wave propagation in general and applies them to tsunami propagation in particular, using analytical models. It is based upon first principles of physics and avoids numerical analysis, which is thus accessible to the broader scientific community. It only requires the knowledge of general science and basic calculus-based physics. The derivations of the relevant equations are relegated to the appendices for quick reference so that the need to search for them outside this article is kept to a minimum.

2. Theory of water waves and tsunamis

The theory of water waves is well-documented in the literature (e.g., Coulson, 1955; Sharman, 1963; Towne, 1967; Elmore & Heald, 1969). The wave velocity of waves on water of density ρ under the action of gravity and surface tension T is obtained from a linear wave equation by ignoring the non-linear term of $\frac{1}{2}v^2$ in Bernoulli's equation (cf. Coulson, 1955; Elmore & Heald, 1969):

$$v = \sqrt{\left(\frac{g}{k} + \frac{Tk}{\rho}\right) \tanh kh} \quad (1)$$

Here h is the depth of water and k the wave number. In terms of the wavelength $\lambda = 2\pi/k$, we have:

$$v = \sqrt{\left(\frac{g\lambda}{2\pi} + \frac{2\pi T}{\lambda\rho}\right) \tanh \frac{2\pi h}{\lambda}} \quad (2)$$

When the gravity and surface tension terms are equal, λ is called the critical wavelength λ_c :

$$\lambda_c = 2\pi \sqrt{\frac{T}{\rho g}} \quad (3)$$

For water waves, $\lambda_c = 1.73$ cm (cf. Towne, 1967; Elmore & Heald, 1969). The corresponding velocity $v_c = 27$ cm/s (Sharman, 1963).

For waves of $\lambda < \lambda_c < h$, the surface tension term dominates and

$$v = \frac{\omega}{k} = \sqrt{\frac{Tk}{\rho}} \quad (4)$$

Thus

$$\omega = \sqrt{\frac{T}{\rho}} k^{3/2} \quad (5)$$

and the group velocity

$$u = \frac{d\omega}{dk} = \frac{3}{2} \sqrt{\frac{Tk}{\rho}} = \frac{3}{2}u \quad (6)$$

The group velocity is faster than the wave velocity! The individual wave-crests fall behind the group while new crests build up at the forward edge of the group (cf. Towne, 1967). Such waves are called *capillary waves* or *ripples*. They are severely attenuated by viscous effects.

For longer wavelengths ($\lambda > \lambda_c$), the gravity term dominates. We have (vide Appendix A):

$$v = \frac{\omega}{k} = \sqrt{\frac{g}{k} \tanh kh} \quad (7)$$

and

$$\omega = \sqrt{gk \tanh kh} \quad (8)$$

Such waves are called *gravity waves*. Customarily, two kinds of gravity waves are recognized depending upon the wavelength $\lambda = 2\pi/k$: (1) If $\lambda > h$, the waves are called *long waves in shallow water*; (2) If $\lambda < h$, the waves are called *short waves in deep water*.

In the first case, $\tanh kh \approx kh$ and the wave velocity

$$v = \sqrt{gh} \quad (9)$$

The group velocity is, from Eq. (8):

$$u = \frac{d\omega}{dk} = \sqrt{gh} = v \quad (10)$$

Owing to the equality of the wave velocity and the group velocity, such waves are non-dispersive.

In the second case, $\tanh kh \approx 1$. Then

$$v = \sqrt{\frac{g}{k}} \quad (11)$$

and from Eq. (8):

$$u = \frac{d\omega}{dk} = \frac{1}{2} \sqrt{\frac{g}{k}} = \frac{1}{2}v \quad (12)$$

In such waves, the individual waves travel faster than the group and rapidly diminish in amplitude as they cross the group (Towne, 1967).

Tsunami waves in the deep ocean typically have wavelengths of about 200 km and velocity of 700 kilometers per hour. They maintain their form in dispersion-less propagation for long

distances with little dissipation of energy. They are thus identified as ‘long waves in shallow water’ even as they travel above the deepest parts of the ocean, the ‘long’ and ‘shallow’ adjectives referring to the relative magnitudes of the wavelength and depth of water. Many of the properties of the tsunamis, such as velocity and dispersion-less propagation follow from this description (e.g., Margaritondo, 2005; Helene & Yamashita, 2006; Tan & Lyatskaya, 2009). However, the linearized theory of water waves is only an approximation to the true situation and a rigorous theory calls for the inclusion of the non-linear term in Bernoulli’s equation. For example, the form of these waves having a narrow crest and very wide trough can only be accounted for by a complete non-linear theory (cf. Elmore & Heald, 1969).

Tsunamis also exhibit the characteristics of ‘canal waves’, first observed by Scott Russell in Scotland in 1834 (Russell, 1844). These disturbances travel like a single wave over long distances and maintain their shapes with little loss of energy. The mathematical theory of such waves, now-a-days called ‘solitary waves’ or ‘solitons’, was developed by Boussinesq (1871), Korteweg & de Vries (1895) and Lord Rayleigh (1914). Their analyses show that in a dispersive medium, the non-linear effect can exactly cancel out the dispersive effect to preserve the form of the wave (cf. Stoker, 1957; Lamb, 1993).

3. Tsunami propagation models

One-dimensional propagation models are the easiest to construct and analyze. Even though they may not represent the real situation for tsunami propagation in the open ocean, valuable results can come out of these models. The ‘long waves in shallow water’ model noted above represents a one-dimensional model (**Model A**) in which the displacement is in the vertical direction and propagation takes place in the horizontal direction (see Appendix A). The Models of Margaritondo (2005) and Helene & Yamashita (2006) are examples of this model. This model correctly predicts the speed of the tsunami by means of Eq. (9). In fact, this equation is widely used in bathymetry. It is also used to calculate the travel times of tsunamis.

In the ‘long waves in shallow water’ model, the group velocity is equal to the wave velocity according to Eqs. (9) and (10). This helps to explain the dispersion-less propagation of the tsunamis. An alternative derivation of these equations is provided by Margaritondo (2005). By assuming that the vertical displacement of water is proportional to distance from the bottom, Margaritondo (2005) arrives at the same result by applying the energy conservation law. As stated earlier, however, a rigorous derivation would call for the solitary wave solution of non-linear differential equation obtained from Navier-Stokes equation (cf. Stoker, 1957).

Eq. (9) has profound consequences in the inundation phase as the tsunami makes landfall. The wave energy density E within a wavelength λ is

$$E \propto A^2 \lambda \propto A^2 v \propto A^2 \sqrt{h} \quad (13)$$

where A is the amplitude of the wave. Assuming E to remain constant, we have

$$A \propto \frac{1}{\sqrt[4]{h}} \quad (14)$$

A 1 m high wave at a depth of 1000 m would become 5.62 m at a depth of 1 m! That goes to illustrate the devastating effects of tsunamis as they make landfall. Helene & Yamashita (2006) have shown that the Eq. (14) holds true when the depth of the ocean floor varies gradually instead of having abrupt steps, which helps the tsunamis to maintain their characteristics as they approach land.

Helene & Yamashita (2006) have further shown how a tsunami will bend dramatically around an obstacle and strike land in the shadow regions. Since $v \propto \sqrt{h}$ according to Eq. (9), the velocity decreases nearer the coast as the depth decreases. The wave-fronts are able to bend dramatically towards the coast in a diffraction pattern and to strike land in the shadow region. This explains the damage caused in the western coasts of Sri Lanka and India during the Boxing day tsunami of December 2004.

Useful as they are, the one-dimensional models of are not appropriate when the tsunami propagates in the open ocean from a well-defined epicenter since the waves will spread out in concentric circles, which calls for two-dimensional models. In **Model B** (Tan & Lyatskaya, 2009), waves propagate outwards on a flat two-dimensional ocean from the epicenter. When the energy conservation principle is imposed, the energy density of the wave falls off inversely as the distance from the epicenter ρ :

$$I_{ModelB} \propto \frac{1}{\rho} \quad (15)$$

The wave amplitude therefore falls off inversely as the square-root of the radial distance ρ :

$$\psi_{ModelB} \propto \sqrt{I_{ModelB}} \propto \frac{1}{\sqrt{\rho}} \quad (16)$$

The formal derivation of the results (15) and (16) are given in Appendix B where it is mentioned that strictly speaking, they apply at distances away from the epicenter.

For long distance propagation, the curvature of the Earth must be taken into consideration. This is incorporated in **Model C** (Tan & Lyatskaya, 2009) which analyzes tsunami propagation on a spherical oceanic surface. In this model, the energy density of the wave varies as (vide Appendix C):

$$I_{ModelC} \propto \frac{1}{\sin \theta} \quad (17)$$

where θ is the zenith angle measured from the center of the Earth with the epicenter at the north pole. Hence the wave amplitude is a function of the polar angle:

$$\psi_{ModelC} \propto \sqrt{I_{ModelC}} \propto \frac{1}{\sqrt{\sin \theta}} \quad (18)$$

The amplitude variation depends solely on the polar angle. Since the epicenter is considered to be located at the north pole ($\theta = 0$), the wave amplitude gradually falls until it reaches the equator ($\theta = \pi/2$), 10,000 km away, and then starts to rise again as the convergence effect due to the curvature of the Earth comes into play and finally regains its original value at the south pole ($\theta = \pi$). Thus, if the Earth were entirely ocean, barring any losses, the wave amplitude would regain its original value at the anti-podal point.

The comparison of wave amplitudes in Model C (true) and Model B (approximate) is given in Appendix C. We have:

$$\frac{\psi_{ModelC}}{\psi_{ModelB}} = \sqrt{\frac{\theta}{\sin\theta}} \quad (19)$$

Table C.1 shows that the difference in the two solutions is slight for small values of θ . Even at the equator ($\theta = \pi/2$), the enhancement in amplitude due to curvature is only 25%. The enhancement becomes progressively greater until the south pole ($\theta = \pi$) is reached, where it becomes infinite.

When the tsunami is caused by an oceanic plate sliding under a continental plate, the subduction zone can be described by a finite line source instead of a localized point source. In that case, **Model D** is appropriate. In this model, the wave-fronts are ellipses with foci at the end-points of the line source and the energy propagates along con-focal hyperbolas (Appendix D). The wave amplitude near the source will be far different from that of a point source (Model B). If c is the length of the line source, then at distances ρ_b from the center across the line source, one has (vide Appendix D):

$$\frac{\psi_{ModelD}}{\psi_{ModelB}} = \frac{1}{\sqrt[4]{1 + \frac{c^2}{\rho_b^2}}} \quad (20)$$

The wave amplitude in Model D is finite at the origin as opposed to being infinite in Models B and C. However, away from the source, the solutions for Models B and D rapidly converge, as the wave-fronts become more circular. For $\rho_b > c$, the difference is below 10%, whereas for $\rho_b > 10c$, the two solutions are virtually indistinguishable (Table D.1).

Tsunamis are vast and highly complex geophysical phenomena, each having a character of its own. It is impossible to construct one model for any tsunami even with a high-speed numerical code. Further, each stage of the tsunami – generation, propagation and inundation, has to be modeled and studied separately. Nonetheless, simplified models based on first principles are able to explain individual aspects of this very complex geophysical phenomenon without detailed numerical computations.

4. Model applications

Viewed from space, the Earth is a watery planet with the oceans covering a full 71% of the surface area. The world ocean consists of three inter-connected oceans of the Pacific, Atlantic

and Indian oceans, which comprise 51.5%, 25.6% and 22.9% of the water surface, respectively (we disregard 'Southern Ocean' as a separate entity). The Pacific ocean is thus larger than the two other oceans put together. It alone covers 34% or just over a full one-third of the Earth's surface and is comfortably larger than all the landmasses (at 29% of the Earth's surface) put together. The Pacific ocean is thought to be the remnant of 'Panthalassa', the world ocean, when all the landmasses were joined together as 'Pangaea'.

The Pacific ocean provides an ideal venue for tsunami propagation studies for several reasons. First, as stated above, it is the largest body of water, covering a full one-third of the globe. Second, it is bounded by active tectonic plate junctions, studded with volcanoes called the 'Ring of Fire'. Tsunamis produced at these hotspots can traverse the length and breadth of the ocean with relative ease. Third, there are no landmasses or large islands to block or interfere with the propagation of tsunamis formed in the ocean. Fourth, the ocean itself is dotted with small islands which pose little interference with tsunami propagation, but provide valuable platforms for recording tsunami wave amplitudes. Many of these islands are volcanic in origin and are sources of tsunamis themselves. Fifth, the longest stretch of ocean water is found between the Japan archipelago in the north-west and southern Chile on the south-east covering a distance of over 17,000 km or 85% of the distance between the North pole and the South Pole. At both the ends of this diameter lie some of the most active plate tectonic regions and tsunamis from either ends have traversed this favorite racetrack. Last but not least, an astonishing 80% of all tsunamis are recorded in the Pacific ocean.

With this geographical backdrop, we now proceed to study representative tsunami event to illustrate the validity of our propagation models. Model A, even though uni-dimensional, is a valuable tool for all tsunami events, as it correctly furnishes the velocity given the depth of the ocean, or vice-versa. It further predicts the travel times, which are vital for warning purposes. These results are independent of the direction, given the isotropy of space. Model A fails when the amplitude of the wave is to be studied, in which case Model B, C or D is called into consideration. In the following, we provide examples where one of the latter models, in conjunction with Model A, is used to analyze historic tsunami events. The data are taken from the National Oceanic and Atmospheric Administration website at www.ngdc.noaa.gov/hazard/tsu_travel_time_events.shtml.

4.1. Hawaii tsunami of 1975

On 29 November 1975, a magnitude 7.2 earthquake occurred on the southern coast of the island of Hawaii with the epicenter at 19.3°N and 155.0°W at a focal depth of 8 km (cf. Pararas-Carayannis, 1976). The earthquake, the largest local one since 1868, generated a locally damaging submarine landslide tsunami which was recorded at 76 tide gauge stations in Alaska, California, Hawaii, Japan, Galapagos Islands, Peru and Chile. The tsunami caused \$1.5 million damage in Hawaii, 2 deaths and 19 injuries (Dudley & Lee, 1988). From the travel times registered, the tsunami reached Guadalupe Island, Mexico, 3864 km away in 5 h 9 m at an average speed of 750 kph, while it took 6 h 8 m to reach Tofino Island, Canada, 4210 km away, at the average speed of 686 kph. The slower speed in the first case is likely to

be due to the fact that the tsunami had to bend considerably before heading towards its destination (cf. Helene & Yamashita, 2006).

Fig. 1 is a scatter plot of the wave amplitude versus the propagation distance. Since the maximum distance was under 8000 km, the flat space approximation holds (vide Appendix C) and Model B is applicable. The variation of the wave amplitude in this model is given by Eq. (16):

$$\psi_{ModelB} = \frac{A}{\sqrt{\rho}} \quad (21)$$

where A is the amplitude constant to be determined by regression analysis. Summing over the data points, one obtains:

$$A = \frac{\sum \psi_{ModelB}}{\sum \frac{1}{\sqrt{\rho}}} \quad (22)$$

The current tsunami data yield: $A = 20.5265$. The model equation is shown in Fig. 1. Also shown in the figure is the actual variation of the wave amplitude in accordance with the data. This is determined by first assuming a functional variation of the form

$$\psi_{observed} = A\rho^\alpha \quad (23)$$

where A and α are two constants to be determined from regression analysis. By taking natural logarithms of both sides first and then multiplying both sides by ρ , we get the two normal equations required to find the constants:

$$\log \psi = \log A + \alpha \log \rho \quad (24)$$

and

$$\rho \log \psi = \rho \log A + \alpha \rho \log \rho \quad (25)$$

By summing Eqs. (24) and (25) over the n data points, we get:

$$\sum \log \psi = n \log A + \alpha \sum \log \rho \quad (26)$$

and

$$\sum \rho \log \psi = \log A \sum \rho + \alpha \sum \rho \log \rho \quad (27)$$

By eliminating A between Eqs. (26) and (27), we have

$$\alpha = \frac{\sum \rho \sum \log \psi - n \sum \rho \log \psi}{\sum \rho \sum \log \rho - n \sum \rho \log \rho} \quad (28)$$

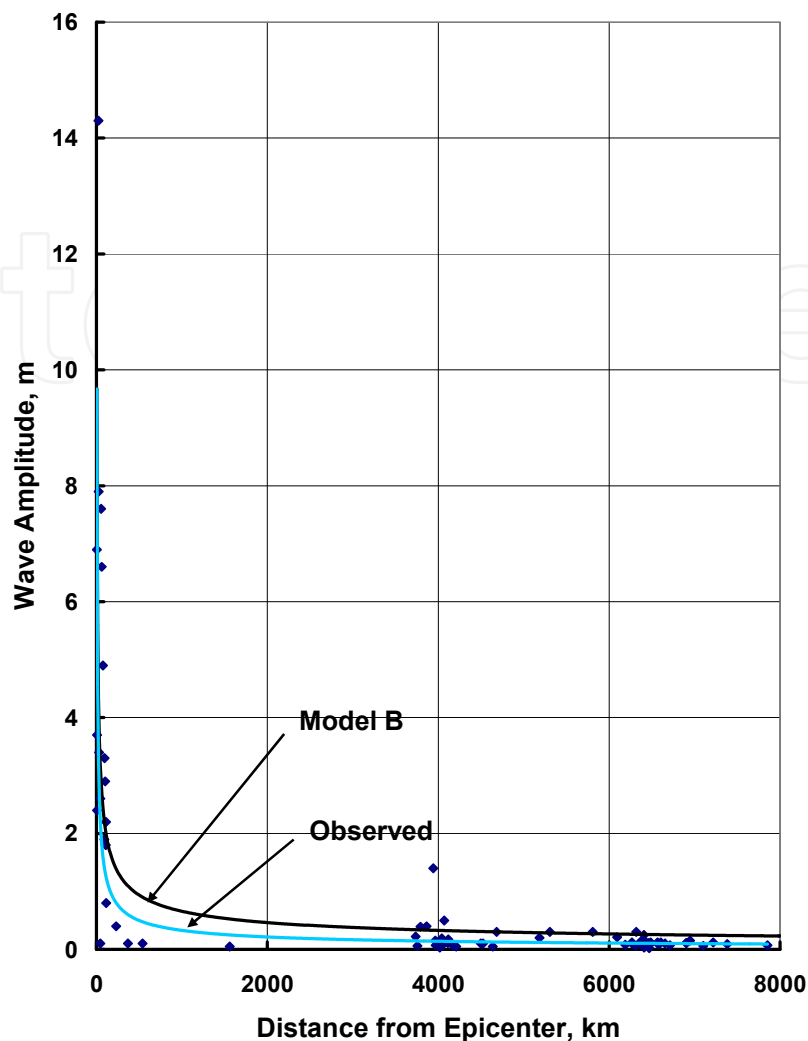


Figure 1. Observed and Model wave amplitudes of Hawaii tsunami of 1975.

A is then obtained from Eq. (23). The results give: $A = 22.644$; and $\alpha = -.6137$. The actual variation of the wave amplitude with distance is then expressed as:

$$\psi_{\text{Observed}} = \frac{22.644}{\rho^{.6137}} \quad (29)$$

The actual wave amplitude falls off slightly faster than that predicted by Model B, which is based on conservation of energy. The difference may be assumed to represent the loss of energy due to as yet unidentified causes. The prime candidate appears to be the generation of atmospheric internal gravity waves by tsunamis, which can transport energy and momentum vertically through the atmosphere and produce travelling ionospheric disturbances (cf. Hickey, 2011). Assuming an exponential attenuation factor, we can write (vide Appendix B)

$$\psi_{\text{Observed}} = e^{-\beta\rho} \psi_{\text{ModelB}} \quad (30)$$

The attenuation factor then follows as

$$e^{-\beta\rho} = \frac{\psi_{Observed}}{\psi_{ModelB}} = \rho^{.5-\alpha} \quad (31)$$

The attenuation factor and the attenuation coefficient are calculated for this event as functions of the distance from the epicenter and entered in Table 1. It shows that the amplitude loss is most rapid near the epicenter with almost 50% of it dissipated in the first 400 km. The dissipation slows down dramatically thereafter and at 10,000 km, it is increases only to 65%. Consequently, the attenuation coefficient is not a constant but a function of the distance from the epicenter. By all accounts, the attenuation is small, suggesting the validity of models A and B.

Distance from epicenter ρ	Attenuation factor $\rho^{.1137}$	Attenuation coefficient β
200 km	.5475	.00301/km
400 km	.5060	.00170/km
600 km	.4832	.00121/km
800 km	.4676	.000950/km
1,000 km	.4559	.000785/km
2,000 km	.4214	.000432/km
4,000 km	.3894	.000236/km
6,000 km	.3719	.000165/km
8,000 km	.3599	.000128/km
10,000 km	.3509	.000105/km

Table 1. Attenuation factor and attenuation coefficient as functions of distance from epicenter

4.2. The Great Japan tsunami of 2011

The Japan archipelago is one of the most earthquake-prone regions of the world. On 11 March 2011, a 9.0 magnitude earthquake struck on the east coast of Honshu. The epicenter was at 38.322°N latitude and 142.369°E longitude, 72 km east of Oshika peninsula with the hypocenter at a depth of 32 km below sea level (cf. <http://www.tsunamiresearchcenter.com/news/earthquake-and-tsunami-strikes-japan>; <http://itic.ioc-unesco.org/index.php>). It was the greatest earthquake to strike Japan and one of the greatest in recorded history. It was comparable to the 2004 Indian Ocean earthquake. There were an estimated 16,000 deaths, 27,000 injured and 3,000 missing (http://www.npa.go.jp/archive/keibi/higaijokya_e.pdf) with total property damage of \$235 billion (according to World Bank reports), making it the costliest natural disaster of all time.

Fig. 2 provides a geometrical perspective of the 2011 Japan tsunami. The geodesic lines from the epicenter shown in the figure are great circles with a longitudinal separation of 90°, which define a ‘lune’ that covers one quarter of the Earth’s surface area. Intersecting the great circles are ‘circles of latitude’ at angular distances of $\theta = \pi/4, \pi/2$ and $3\pi/4$ which

translate to linear distances of 5,000 km, 10,000 km, and 15,000 km, respectively, from the epicenter. For constant propagation speeds, the circles of latitude define circular wavefronts. The 10,000 km great circle marks the 'equator' ($\theta = \pi/2$), past which the waves begin to converge according to Model C. A tsunami propagating in this lune does not encounter any continental landmass until after a distance of 17,000 km, which is 85% of the distance between the poles.



(adapted from worldatlas.com).

Figure 2. Propagation geometry of 2011 Japan tsunami in a lune of angle 90° with wavefronts at intervals of 5,000 km

The 2011 Japan tsunami was felt throughout the Pacific Ocean. Wave amplitudes were recorded at over 293 stations scattered in and around the Pacific. Fig. 3 is a scatter plot of the wave amplitude versus the distance from the epicenter. The highest amplitudes were recorded near the epicenter. Amidst a considerable scatter, a well-defined trend in the wave amplitudes emerges from the figure. The wave amplitude diminished rapidly as a function of the distance from the source, becoming nearly constant around the 10,000 km mark, and showing a discernible rise thereafter in accord with Model C. But for the intervention of the South American landmass, the waves would have converged at the anti-podal point in south Atlantic Ocean, and barring losses, the original wave amplitude restored.

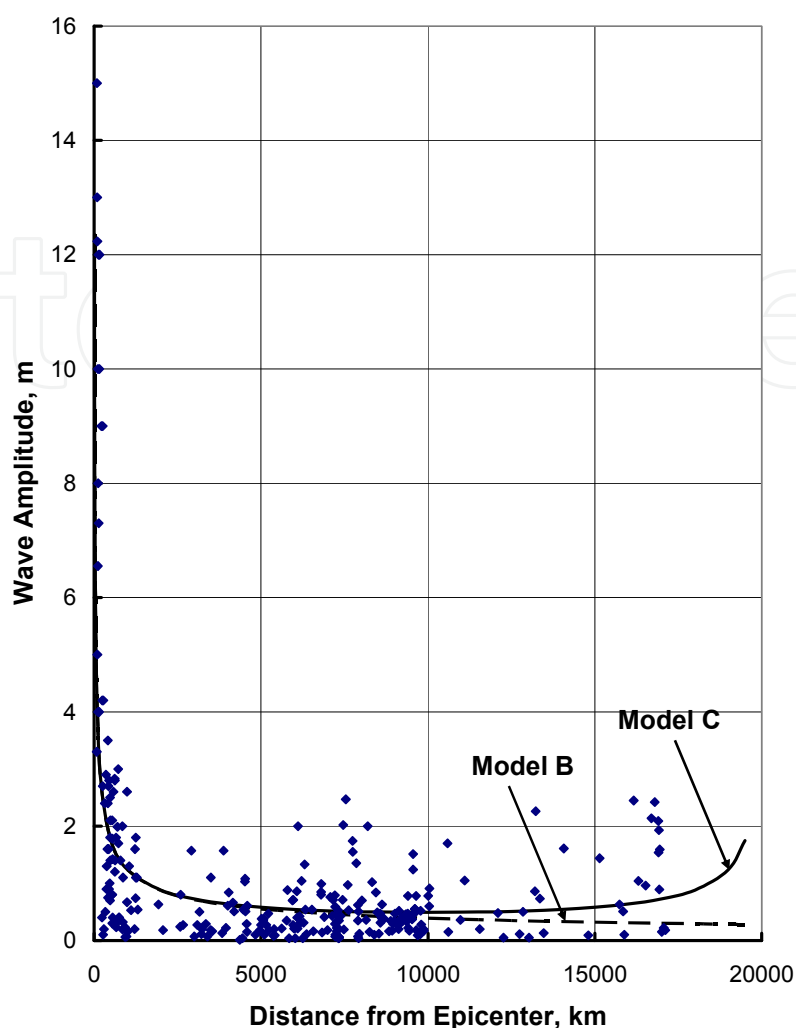


Figure 3. Observed wave amplitudes of 2011 Japan tsunami with least-squares error lines according to Models B and C.

The variation of the wave amplitude according to Model C can be written as [from Eq. (18)]:

$$\psi_{ModelC} = \frac{A}{\sqrt{\sin \theta}} \quad (32)$$

where A is a constant to be determined from the data. In terms of the radial distance ρ , we have

$$\psi_{ModelC} = \frac{A}{\sqrt{\alpha \sin \rho}} \quad (33)$$

where ρ is in kilometers and $\alpha = .009$ deg/km or $.00015708$ /km if θ is expressed in radian measure.

The constant A is determined from a single normal equation obtained by summing over the n observed data points

$$A = \sqrt{\frac{\sum \psi_{ModelC}^2 \sin \alpha \rho}{n}} \quad (34)$$

giving $A = .4896$ m. The least-square error line according to Model C is then given by Eqs. (33) and (34). The same in Model B is obtained by Eq. (19):

$$\psi_{ModelB} = \sqrt{\frac{\sin \alpha \rho}{\alpha \rho}} \psi_{ModelC} \quad (35)$$

The regression lines according to Models B and C are superimposed on the data points in Fig. 3. As is shown in Appendix C, the difference between the two wave amplitudes is slight up to about the equator mark (10,000 km), after which the two curves begin to diverge. The predicted amplitude in Model B continues to fall according to Eq. (21), whereas that in Model C begins to rise according to Eqs. (32) and (33). The actual data clearly supports Model C and validates the convergence effect of the Earth's curvature on the wave amplitude. The same effect was earlier observed in the 8.3 magnitude Kuril islands earthquake of 2006 (Tan & Lyatskaya, 2009).

Finally, Eq. (9) of Model A furnishes a means to determine the average depth of the ocean along the travel path given the distance and the travel time to the destination:

$$d = \frac{v^2}{g} \quad (36)$$

From the observed travel times and the geodesic distances from the epicenter to 13 destinations along the coast of Chile, the average travel speeds were calculated from which the average depth of the ocean along the travel path determined (Table 2). The mean average speed of 739 kph yielded a mean average depth of 4303 m for the Pacific Ocean along these paths, which compares favorably with various estimates found in the literature: e.g., 4282 m (Herring & Clarke, 1971), 4190 m (Smith & Demopoulos, 2003), 4267 m (<http://oceanservice.noaa.gov>), and 4080 m (britannica online encyclopedia).

The average depth of the Pacific Ocean (4300 m) is considerably greater than those of the Atlantic Ocean (3600 m) and Indian Ocean (3500 m) (cf. Herring & Clarke, 1971). Further, the smaller north-western half of the Pacific Ocean is substantially deeper than the larger south-eastern remainder, even though separate depth figures are hard to find in the literature. In order to estimate the average depth of north-western Pacific Ocean, we consider the travel times of the tsunami to reach various destinations on the coasts of the Hawaiian islands, which lie entirely in that region (Table 3). Travel time data from the epicenter to 8 destinations in the Hawaiian islands yield a mean average speed of 798 kph for a mean average depth of 5016 m for north-western Pacific Ocean along these paths. This confirms the fact that north-western Pacific Ocean is considerably deeper than the south-eastern remainder. These travel time studies further re-affirm the validity of the 'long wave in shallow water' approximation for tsunami propagation.

Latitude of Destination	Destination	Distance from Epicenter	Travel Time	Average Speed	Mean Average Speed	Average Depth	Mean Average Depth
18.467°S	Arica	16,166 km	21 h 26 m	754 kph	739 kph	4,479 m	4,303 m
20.217°S	Iquique	16,308 km	21 h 18 m	766 kph		4,615 m	
23.650°S	Antofagasta	16,522 km	21 h 33 m	767 kph		4,628 m	
27.067°S	Caldera	16,693 km	21 h 44 m	768 kph		4,645 m	
29.933°S	Coquimbo	16,799 km	22 h 04 m	761 kph		4,563 m	
33.033°S	Valparaiso	16,911 km	22 h 13 m	761 kph		4,562 m	
33.583°S	San Antonio	16,932 km	22 h 11 m	763 kph		4,587 m	
35.356°S	Constitucion	16,921 km	23 h 08 m	731 kph		4,213 m	
36.683°S	Talcahuano	16,905 km	22 h 57 m	737 kph		4,272 m	
39.867°S	Corral	16,946 km	22 h 54 m	740 kph		4,312 m	
41.483°S	P. Montt	17,006 km	25 h 20 m	671 kph		3,548 m	
45.467°S	72.339°W	17,065 km	25 h 06 m	680 kph		3,639 m	
54.933°S	P. Williams	17,115 km	24 h 05 m	711 kph		3,976 m	

Table 2. Travel Times, Average Speed and Average Depth of Pacific Ocean.

Latitude of Destination	Destination	Distance from Epicenter	Travel Time	Average Speed	Mean Average Speed	Average Depth	Mean Average Depth
21.960°N	Kauai	5,792 km	7 h 10 m	808 kph	798 kph	5,143 m	5,016 m
21.437°N	Mokuoloe	5,961 km	7 h 32 m	791 kph		4,930 m	
21.300°N	Honolulu	5,962 km	7 h 27 m	800 kph		5,042 m	
20.898°N	Maui	6,108 km	7 h 40 m	797 kph		4,998 m	
20.780°N	Lanai	6,071 km	7 h 48 m	778 kph		4,770 m	
20.036°N	Kawaihae	6,217 km	7 h 48 m	797 kph		5,002 m	
19.733°N	Hilo	6,302 km	7 h 56 m	794 kph		4,968 m	
19.634°N	156.507°W	6,182 km	7 h 33 m	819 kph		5,279 m	

Table 3. Travel Times, Average Speed and Average Depth of north-western Pacific Ocean.

4.3. The Great Chilean tsunami of 1960

On Sunday, May 22, 1960, at 19:11 GMT (15.11 LT), a super-massive earthquake occurred off the coast of south central Chile, with epicenter at 39.5°S latitude, 74.5°W longitude and focal depth of 33 km (cf. http://earthquake.usgs.gov/earthquakes/world/events/1960_05_22_tsunami.php). It happened when a piece of the Nazca Plate of the Pacific Ocean subducted beneath the South American Plate. The magnitude of the earthquake of 9.5 makes it the most powerful earthquake in recorded history (Kanamori, 2010). The tsunami generated by the earthquake, along with coastal subsidence and flooding, caused tremendous damage along the Chilean coast where an estimated 2,000 people lost their lives

(http://neic.usgs.gov/neis/eq_depot/world/1960_05_22articles.html). The resulting tsunami raced across the Pacific Ocean causing the death of 61 people in Hawaii and 200 others in Japan and elsewhere (USGS reports). The estimated damage costs were near half a billion dollars.



(adapted from worldatlas.com).

Figure 4. Propagation geometry of 1960 Chilean tsunami in a lune of angle 90° with wavefronts at intervals of 5,000 km

The Great Chilean tsunami of 1960 is similar to the Great Japan tsunami of 2011 coming from the opposite direction, only having greater amplitude. Both of these tsunamis, as well as many other analogous ones, traversed the longest stretch of continuous water covering over 85% of the distance between the poles. Thus the amplitude variations with distance of both of these tsunamis were similar. The strength of the Great Chilean tsunami was such that reflected waves from the Asian coasts were detectable (<http://www.soest.hawaii.edu/GG/ASK/chile-tsunami.html>).

Fig. 4 provides the geometrical perspective of the 1960 Chilean tsunami. As in the earlier example, the geodesic lines from the epicenter shown in the figure are great circles with a longitudinal separation of 90° , which define a 'lune' that covers one quarter of the Earth's surface area. Intersecting the great circles are 'circles of latitude' at angular distances of $\theta = \pi/4, \pi/2$ and $3\pi/4$ which translate to linear distances of 5,000 km, 10,000 km, and 15,000 km,

respectively, from the epicenter. For constant propagation speeds, the circles of latitude define circular wavefronts. The 10,000 km great circle marks the ‘equator’ ($\theta = \pi/2$), past which the waves begin to converge according to Model C.

The Great Chilean tsunami of 1960 was felt throughout the Pacific Ocean. Over 1,000 measurements of wave amplitudes were recorded at 815 stations scattered in and around the Pacific. Fig. 5 is a scatter plot of the wave amplitude versus the distance from the epicenter. The highest amplitudes were recorded near the Chilean coast and at the diametrically opposite end, mostly on the Japanese coasts, where hundreds of data points were clustered. There is a second cluster past the 10,000 km mark at the Hawaiian Islands, where numerous measurements were taken. The over-all trend of the data points closely agrees with that predicted by the ‘spherical ocean’ Model C.

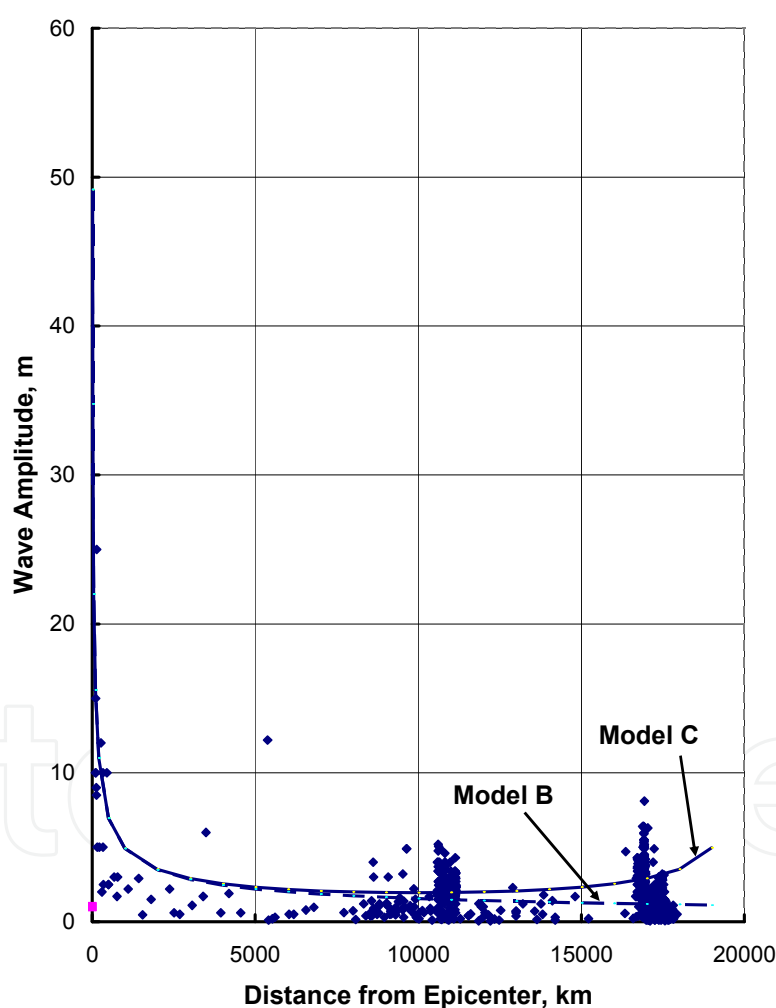


Figure 5. Observed wave amplitudes of 1960 Chilean tsunami with least-squares error lines according to Models B and C.

The least-squares regression lines of the data points as obtained from Eqs. (32) - (35) are shown in Fig. 5, with the amplitude constant $A = 1.9488$ m. This is 3.98 times that of the 2011 Japan tsunami constant. Since the energy density of the waves is proportional to A^2 , this

indicates that the energy density of the 1960 Chilean tsunami was 15.84 times that of the 2011 Japan tsunami, thus illustrating the power of the most powerful earthquake in recorded history. Normally, a 9.5 magnitude earthquake releases about 5.5 times the energy as a 9.0 earthquake (cf. Kanamori, 1977).

From the observed travel times and distances from the epicenter to destinations on the eastern coast of Japan, the average travel speeds were calculated and the average depth of the ocean determined along these paths (table 4). The mean average depth of 4,231 m compares favorably with the value of 4,303 m obtained from the 2011 Japan tsunami (Table 2). Also calculated were the travel speeds from the epicenter to locations on the Hawaiian Islands and the average depth of the ocean (Table 5). The mean average depth of 3,972 m reaffirms the fact that the north-western Pacific Ocean, at 5,016 m (Table 3) is substantially deeper than its south-eastern complement.

Latitude of Destination	Destination	Distance from Epicenter	Travel Time	Average Speed	Mean Average Speed	Average Depth	Mean Average Depth
41.783°N	Hakodate	17,058 km	23 h 27 m	727 kph	733 kph	4,166 m	4,231 m
39.267°N	Kamaishi	16,914 km	22 h 24 m	755 kph		4,489 m	
35.670°N	Tokyo	16,989 km	22 h 59 m	739 kph		4,302 m	
28.383°N	Nase	17,496 km	24 h 39 m	710 kph		3,967 m	

Table 4. Travel Times, Average Speed and Average Depth of Pacific Ocean

Latitude of Destination	Destination	Distance from Epicenter	Travel Time	Average Speed	Mean Average Speed	Average Depth	Mean Average Depth
19.730°N	Coconut I.	10,621 km	15 h 30 m	685 kph	710 kph	3,697 m	3,972 m
19.733°N	Hilo	10,621 km	14 h 47 m	718 kph		4,064 m	
20.898°N	Kahului	10,817 km	15 h 07 m	716 kph		4,032 m	
21.300°N	Honolulu	10,957 km	15 h 22 m	713 kph		4,003 m	
28.960°N	Nawiliwili	11,124 km	15 h 29 m	718 kph		4,064 m	

Table 5. Travel Times, Average Speed and Average Depth of south-eastern Pacific Ocean

4.4. The Great Indian Ocean tsunami of 2004

The great 2004 Indian Ocean earthquake occurred off the west coast of Sumatra, Indonesia, on Boxing Day, December 26, 2004. Its revised magnitude of 9.2 makes it the second largest earthquake in recorded history, after the 9.5 magnitude Chilean earthquake of 1960 (cf. <http://walrus.usgs.gov/tsunami/sumatraEQ/>; Lay, et al., 2005). In terms of human casualties, however, it was the greatest natural disaster in recorded history, by far. The earthquake generated a super-massive tsunami that took the lives of an estimated 230,000

people in Indonesia, Sri Lanka, India, Thailand and elsewhere (Mörner, 2010). More than 1,000,000 people were displaced in the aftermath following the tsunami, which was eventually registered at every coast of the world ocean.



Figure 6. Propagation geometry of 2004 Indian Ocean tsunami showing the two major faultlines and propagation along their perpendicular bisectors (adapted from phuket.news.com).

This great earthquake was caused by the subduction of the Indo-Australian plate under the Eurasian plate near the Andaman and Nicobar Islands chain and its extension southwards under the Bay of Bengal (Fig. 6). Its hypocenter is listed at 3.295°N latitude and 95.982°W longitude. However, its fault-line was 1000 km long, which roughly consisted of two linear segments (cf. Kowalik, et al., 2005): (1) a 700 km long section off the west coasts of Andaman and Nicobar Islands; and (2) a 300 km section west of Aceh province of Sumatra, Indonesia (Fig. 6). The alignments of both the segments were generally north-south, with the southern segment tilted slightly towards the south-easterly direction. The shorter southern segment had the more intense earthquake and generated the greater tsunami. Consequently, the epicenter lied on this segment of the fault-line. The earthquake is also variously referred to as the Sumatra-Andaman earthquake or the Boxing Day earthquake.

It is evident from Fig. 6 that the eastward tsunami from the southern segment of the fault-line (henceforth referred to as the Sumatra fault-line) had a direct impact on the Aceh province in northern Sumatra, where the highest waves of over 50 m were registered. More than half of all casualties were reported there. The westward tsunami from this fault-line, on the other hand, passed harmlessly over the open ocean, reaching the east coast of South

Africa, and entering the Atlantic Ocean. The northern segment of the fault-line (henceforth called the Andaman-Nicobar fault-line) produced tsunami which affected greater areas of landmass. Phuket lied near the perpendicular bisector of this fault and took a direct hit from the tsunami as did other coastal locations of Thailand and Myanmar. To the west, the east coasts of Sri Lanka and southern India were greatly affected. The tsunami rolled over the Maldiv Islands and reached the eastern coast of Africa (Somalia, in particular), causing damage there. In consolation, Bangladesh, a densely populated area to the north, was spared the devastation.

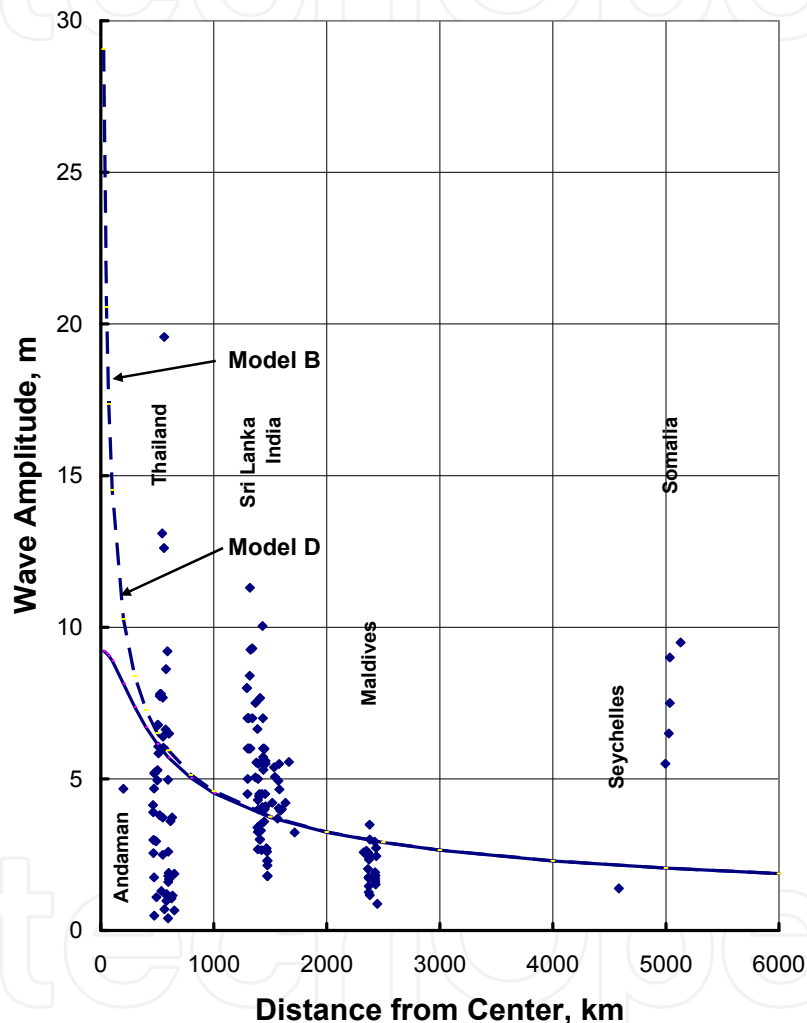


Figure 7. Observed and Model wave amplitudes of 2004 Indian Ocean earthquake due to the Andaman-Nicobar fault-line.

Assuming that the tsunami from the Sumatra fault-line was largely intercepted by the island (vide Fig. 6), we proceed to analyze the tsunami propagation from the Andaman-Nicobar fault-line based on Models B and D. For this, we have to consider the mid-point of the fault-line (approximately 9°N latitude and 92.5°E longitude) as the origin of the tsunami instead of the epicenter which lay on the Sumatra fault-line. Distances are now reckoned from this new center. If the coordinates (latitude, longitude) of the source and destination points be

(λ_s, ϕ_s) and (λ_d, ϕ_d) , respectively, the angle subtended at the center of the Earth by the two locations is, from spherical trigonometry,

$$\theta = \cos^{-1} \left[\sin \lambda_s \sin \lambda_d + \cos \lambda_s \cos \lambda_d \cos(\phi_d - \phi_s) \right] \quad (37)$$

The linear distance between the two points on the surface of the Earth is then $d = \theta r_e$, where $r_e = 6371$ km, is the volumetric radius of the Earth prescribed by the International Union of Geodesy and Geophysics.

Fig. 7 is a scatter plot of the wave amplitudes as functions of the distance from the center of the Andaman-Nicobar fault-line. The data betray distinct clumps for Thailand, Sri Lanka, India and Maldives. At the far end are data for the Somalia coast. Also shown are the isolated data points for Andaman and Seychelles islands. Superimposed on the data points are the model amplitudes according to Models B and D. The model amplitudes are virtually indistinguishable for distances upwards of 1000 km (cf. Appendix D). In comparison with the Hawaii and Japan earthquakes (Figs. 1 and 3), the wave amplitudes are significantly higher, which is indicative of the magnitude of the earthquake. Unlike Hawaii and Japan earthquakes, however, there is a dearth of data points with high amplitudes near the origin. This is because the earthquake occurred beneath the ocean and there was no land close to it. Nevertheless, the lack of high wave amplitudes close to the fault-line appears to support the validity of Model D.

As before, the wave amplitudes according to Model B is given by (vide Eq. D.12):

$$\psi_{ModelB} = \frac{A}{\sqrt{\rho_b}} \quad (38)$$

where A is a constant to be determined from regression analysis of the data points. By summing over the data, we have

$$A = \frac{\sum \psi}{\sum \frac{1}{\sqrt{\rho_b}}} \quad (39)$$

The data yield a value of $A = 146.296$ m. The wave amplitudes in accordance with Model D then follows (vide Eq. D.8):

$$\psi_{ModelD} = \frac{\psi_{ModelB}}{\sqrt[4]{1 + \frac{c^2}{2\rho_b^2}}} \quad (40)$$

Here $c = 350$ km.

From the travel times and the travel distances from the epicenter on the Sumatra fault-line to five destinations on the South African coast and one on the Antarctic coast, the average

speed of the tsunami was calculated, and the average depth of the Indian Ocean determined (Table 6). The average speed of 700 kph translates to an average depth of 3,840 m which is quite consistent with the reference figure of 3,963 m found in the literature (Herring & Clarke, 1971). Once again, the tsunami speed and depth of the ocean predicted by the 'long waves in shallow water' model turns out to be reliable.

Latitude of Destination	Destination	Distance from Epicenter	Travel Time	Average Speed	Mean Average Speed	Average Depth	Mean Average Depth
28.800°S	Richards Bay	7,683 km	11 h 04 m	694 kph	700 kph	3,795 m	3,840 m
33.027°S	East London	8,193 km	11 h 29 m	713 kph		4,008 m	
33.958°S	Pt. Elizabeth	8,423 km	12 h 13 m	698 kph		3,743 m	
34.178°S	Mossel Bay	8,743 km	13 h 02 m	671 kph		3,543 m	
34.188°S	Simons Bay	9,078 km	12 h 53 m	705 kph		3,909 m	
69.007°S	39.584°E	9,088 km	12 h 41 m	717 kph		4,042 m	

Table 6. Travel Times, Average Speed and Average Depth of Central Indian Ocean

5. Conclusion

Tsunamis are complex geophysical phenomena not easily amenable to theoretical rendering. The formal theory based on solitary wave model is not easily accessible to the great majority of the scientific readers. This chapter has demonstrated that the 'long waves in shallow water' approximation of the tsunami explains many facets of tsunami propagation in the open ocean. The one-dimensional model provides accurate assessments of the general properties such as dispersion-less propagation, speed of propagation, bending of tsunamis around obstacles and depth of the ocean, among others. Two-dimensional models on flat and spherical ocean substantially account for the wave amplitudes for far-reaching tsunami propagation. Finally, the finite line-source model satisfactorily predicts the wave amplitudes near the source when the tsunami is caused by a long subduction zone.

Appendix

A. Propagation of water waves in one dimension

A wave is a transfer of energy from one part of a medium to another, the medium itself not being transported in which process (e.g., Coulson, 1955). The individual particles of the medium execute simple harmonic motions in one or two dimensions, depending upon the nature of the wave. For sound waves in air, the oscillations are parallel with the direction of propagation. Such waves are called *longitudinal waves*. For waves along a stretched string, the oscillations are perpendicular to the direction of propagation. Such waves are called *transverse waves*. Longitudinal waves can propagate through solids and fluid media (liquid or gas), whereas transverse waves can propagate through solids only. Longitudinal waves

are sustained by compression forces, while transverse waves are due to shear forces. The sources of all waves are vibrations of some kinds.

In an earthquake, as many as four kinds of waves are produced, of which two are *body waves* and the other two are *surface waves*. The body waves are categorized as: (1) Longitudinal waves (called the *primary waves*); and (2) Transverse waves (called *secondary waves*). The surface waves, too, fall into two categories: (1) Transverse waves called *Love waves*, where the oscillations are parallel with the surface but perpendicular to the direction of propagation; and (2) *Rayleigh waves*, in which the oscillations take place in directions both parallel with and perpendicular to the direction of propagation, the latter taking place in the vertical direction. In Rayleigh waves, the particles below the surface undergo elliptical motions in the vertical plane.

Waves on the surface of water are similar to the Rayleigh waves. They are influenced by three physical factors: (1) *Gravitation*, which acts to return the disturbed surface back to the equilibrium configuration; (2) *Surface Tension*, since the pressure under a curved surface is different from that beneath a flat surface; and (3) *Viscosity*, which causes dissipation of energy. Of these, gravity is the dominant force except in the very short wavelength regions. Water waves controlled by gravity are called *gravity waves*. When surface tension dominates, the waves are called *capillary waves* or *ripples*. Such waves have wavelengths shorter than 1.7 cm and are quickly damped out by viscous forces (cf. Towne, 1967; Elmore & Heald, 1969).

The theory of gravity wave propagation in one dimension is well documented in the literature. A particularly elegant treatment is found in Elmore & Heald (1969). Conventionally, x is taken as the direction of propagation and y is taken to be the vertical direction. The conditions are assumed to be uniform in the z direction, which then disappears from the view of analysis. As water is an incompressible fluid, its density ρ is constant. The equation of continuity gives

$$\vec{\nabla} \cdot \vec{v} = 0 \quad (\text{A.1})$$

where $\vec{v} = v_x \hat{x} + v_y \hat{y}$ represents the velocity. Also, for irrotational motion, we have

$$\vec{\nabla} \times \vec{v} = \vec{0} \quad (\text{A.2})$$

According to the potential theory, \vec{v} is obtained from a velocity potential:

$$\vec{v} = -\vec{\nabla} \phi \quad (\text{A.3})$$

where ϕ is a scalar function which satisfies Laplace's equation:

$$\nabla^2 \phi = \frac{\partial^2 \phi}{\partial x^2} + \frac{\partial^2 \phi}{\partial y^2} = 0 \quad (\text{A.4})$$

If ξ and η represent the displacements in the horizontal and vertical directions, respectively, then

$$v_x = \frac{\partial \xi}{\partial t} = -\frac{\partial \phi}{\partial x} \quad (\text{A.5})$$

and

$$v_y = \frac{\partial \eta}{\partial t} = -\frac{\partial \phi}{\partial y} \quad (\text{A.6})$$

At the bottom, the vertical component of velocity must vanish:

$$v_y = -\frac{\partial \phi}{\partial y} = 0, \quad y = 0 \quad (\text{A.7})$$

At the surface of water, the pressure is atmospheric pressure P . Omitting the non-linear term $\frac{1}{2}v^2$ in Bernoulli's equation, we can write

$$P + \rho g(h + \eta) = \rho \frac{\partial \phi}{\partial t} + \text{const.}, \quad y = h \quad (\text{A.8})$$

where h is the depth of water and g the acceleration due to gravity. Eq. (A.8) constitutes the relation between the variation of pressure due to the vertical displacement of water and the resulting change in the velocity potential. Differentiating Eq. (A.8) with respect to t , we get

$$v_y = \frac{\partial \eta}{\partial t} = \frac{1}{g} \frac{\partial^2 \phi}{\partial t^2} \quad (\text{A.9})$$

Our task now is to find the velocity potential which satisfies Laplace's equation (A.4) and the two boundary conditions (A.7) and (A.9). We assume a trial solution

$$\phi(x, y, t) = X(x)Y(y)T(t) \quad (\text{A.10})$$

and apply the method of separation of variables. From Eq. (C.4), we get

$$\frac{1}{X} \frac{d^2 X}{dx^2} = -\frac{1}{Y} \frac{d^2 Y}{dy^2} = -k^2 \quad (\text{A.11})$$

where the separation constant k is chosen to insure that X is a periodic function of x . Written separately, Eq. (A.11) gives

$$\frac{d^2 X}{dx^2} + k^2 X = 0 \quad (\text{A.12})$$

and

$$\frac{d^2 Y}{dy^2} - k^2 Y = 0 \quad (\text{A.13})$$

The general solutions to Eqs. (A.12) and (A.13) are, respectively

$$X(x) = Ae^{ikx} + Be^{-ikx} \quad (\text{A.14})$$

and

$$Y(y) = Ce^{ky} + De^{-ky} \quad (\text{A.15})$$

For a wave travelling in the forward direction, $B = 0$. Further, from Eq. (A.10):

$$\frac{\partial \phi}{\partial y} = XT \frac{dY}{dy} \quad (\text{A.16})$$

The boundary condition at the bottom (A.7) dictates that $C = D$. Thus

$$Y(y) = 2C \cosh ky \quad (\text{A.17})$$

and

$$\phi(x, y, t) = A \cosh kye^{ikx}T(t) \quad (\text{A.18})$$

where A is a new arbitrary constant. Now from Eqs. (A.6) and (A.9), we get:

$$v_y = -\frac{\partial \phi}{\partial y} = -kA \sinh kye^{ikx}T(t) \quad (\text{A.19})$$

and

$$v_y = \frac{1}{g} \frac{\partial^2 \phi}{\partial t^2} = \frac{1}{g} A \cosh kye^{ikx} \frac{d^2 T(t)}{dt^2} \quad (\text{A.20})$$

Eqs. (A.19) and (A.20) yield:

$$\frac{d^2 T}{dt^2} + (gk \tanh kh)T = 0 \quad (\text{A.21})$$

Hence, the velocity potential has a simple harmonic time-dependence with angular frequency

$$\omega = \sqrt{gk \tanh kh} \quad (\text{A.22})$$

If we choose $T = e^{-i\omega t}$, the velocity potential of a gravity wave propagating in the forward x direction over water of depth h becomes

$$\phi = A \cosh kye^{i(kx - \omega t)} \quad (\text{A.23})$$

The wave velocity of the gravity wave is thus

$$v = \frac{\omega}{k} = \sqrt{\frac{g}{k} \tanh kh} \quad (\text{A.24})$$

B. Wave propagation on two-dimensional flat surface

The equation of a wave emanating from a point source in a two-dimensional plane is conveniently expressed in plane polar coordinates (ρ, ϕ) with the source at the origin (e.g., Zatzkis, 1960):

$$\frac{\partial^2 \psi}{\partial \rho^2} + \frac{1}{\rho} \frac{\partial \psi}{\partial \rho} + \frac{1}{\rho^2} \frac{\partial^2 \psi}{\partial \phi^2} = \frac{1}{v^2} \frac{\partial^2 \psi}{\partial t^2} \quad (\text{B.1})$$

where v is the velocity of the wave. Assuming circular symmetry (i.e., ψ independent of ϕ), we get:

$$\frac{\partial^2 \psi}{\partial \rho^2} + \frac{1}{\rho} \frac{\partial \psi}{\partial \rho} = \frac{1}{v^2} \frac{\partial^2 \psi}{\partial t^2} \quad (\text{B.2})$$

To apply the method of separation of variables, let

$$\psi(\rho, t) = P(\rho)T(t) \quad (\text{B.3})$$

Then Eq. (B.2) becomes

$$T \frac{d^2 P}{d\rho^2} + \frac{T}{\rho} \frac{dP}{d\rho} = \frac{P}{v^2} \frac{d^2 T}{dt^2} \quad (\text{B.4})$$

Dividing both sides by ψ , separating the variables, and letting each side equal to a constant ($-k^2$), we get

$$\frac{1}{P} \frac{d^2 P}{d\rho^2} + \frac{1}{P\rho} \frac{dP}{d\rho} = \frac{1}{v^2 T} \frac{d^2 T}{dt^2} = -k^2 \quad (\text{B.5})$$

The t -equation is

$$\frac{d^2 T}{dt^2} + k^2 v^2 T = 0 \quad (\text{B.6})$$

whose solution is

$$T \propto e^{\pm i k v t} \quad (\text{B.7})$$

The ρ -equation is

$$\rho^2 \frac{d^2 P}{d\rho^2} + \rho \frac{dP}{d\rho} + k^2 \rho^2 P = 0 \quad (\text{B.8})$$

or

$$\rho \frac{d}{d\rho} \left(\rho \frac{dP}{d\rho} \right) + k^2 \rho^2 P = 0 \quad (\text{B.9})$$

This is Bessel's equation of the zeroth order. A novel technique to solve this equation is found in Irving & Mullineaux (1959). Let

$$P = \frac{R}{\sqrt{\rho}} \quad (\text{B.10})$$

Then Eq. (B.9) assumes the form

$$\frac{d^2 R}{d\rho^2} + k^2 \left[1 + \frac{1}{4k^2 \rho^2} \right] R = 0 \quad (\text{B.11})$$

For large ρ (i.e., away from the source), the second term within the square bracket may be neglected. Thus

$$\frac{d^2 R}{d\rho^2} + k^2 R = 0 \quad (\text{B.12})$$

giving the solution

$$R \propto e^{ik\rho} \quad (\text{B.13})$$

Hence, from Eq. (B.10):

$$P \propto \frac{e^{ik\rho}}{\sqrt{\rho}} \quad (\text{B.14})$$

and

$$\psi(\rho, t) = P(\rho)T(t) = \psi_0 \frac{e^{ik(\rho \pm vt)}}{\sqrt{\rho}} \quad (\text{B.15})$$

Since the wave is propagating outwards, we retain the + sign only, giving

$$\psi(\rho, t) = \psi_0 \frac{e^{ik(\rho - vt)}}{\sqrt{\rho}} \quad (\text{B.16})$$

In terms of the wave number k ,

$$\psi(\rho, t) = \psi_0 \frac{e^{i(k\rho - \omega t)}}{\sqrt{\rho}} \quad (\text{B.17})$$

The amplitude of the wave falls off inversely as the square-root of the distance from the source:

$$\psi_{\text{ModelB}} \propto \frac{1}{\sqrt{\rho}} \quad (\text{B.18})$$

The intensity of the wave (i.e., the energy density) is thus inversely proportional to the distance from the source:

$$I_{\text{ModelB}} \propto \psi_{\text{ModelB}}^2 \propto \frac{1}{\rho} \quad (\text{B.19})$$

There is a simple alternative procedure to obtain Eq. (B.18) from Eq. (B.19) (Tan & Lyatskaya, 2009). Assuming conservation of energy, the energy spreads out in concentric circles of radius ρ , so that the intensity of the wave varies inversely as the radial distance whence the wave amplitude varies according to Eq. (B.18).

When k is complex, we can write $k = \kappa + i\beta$, Eq. (B.16) then takes the form

$$\psi(\rho, t) = \psi_0 \frac{e^{-\beta\rho} e^{i(k\rho - \omega t)}}{\sqrt{\rho}} \quad (\text{B.20})$$

In Eq. (B.20), $e^{-\beta\rho}$ gives the attenuation factor when loss processes are present, with β representing the attenuation coefficient.

C. Wave propagation on two-dimensional spherical surface

For long-distance propagation of waves on a spherical surface, the curvature of the surface must be taken into account (Tan & Lyatskaya, 2009). Use spherical coordinates (r, θ, ϕ) with the center of the sphere as the origin and place the source of the wave at the north pole ($\theta = 0$) (Fig. C.1). Assume azimuthal symmetry, i.e., ψ independent of ϕ . Then circular waves will propagate on the surface of the sphere ($r = a$) outwards in the direction of increasing zenith angle θ . The wave-fronts will be small circles on the sphere having radii $a\sin\theta$ and circumferences $2\pi a\sin\theta$. The energy conservation principle now requires that the intensity of the wave varies inversely as $\sin\theta$:

$$I_{\text{ModelC}} \propto \psi^2 \propto \frac{1}{\sin\theta} \quad (\text{C.1})$$

Hence the amplitude of the wave varies inversely as the square-root of $\sin\theta$:

$$\psi_{\text{ModelC}} \propto \frac{1}{\sqrt{\sin\theta}} \quad (\text{C.2})$$

The amplitude and intensity of the wave decrease from the north pole ($\theta = 0$) to the equator ($\theta = \pi/2$), but increase thereafter until the wave converges at the south pole ($\theta = \pi$), where the original amplitude and intensity are restored.

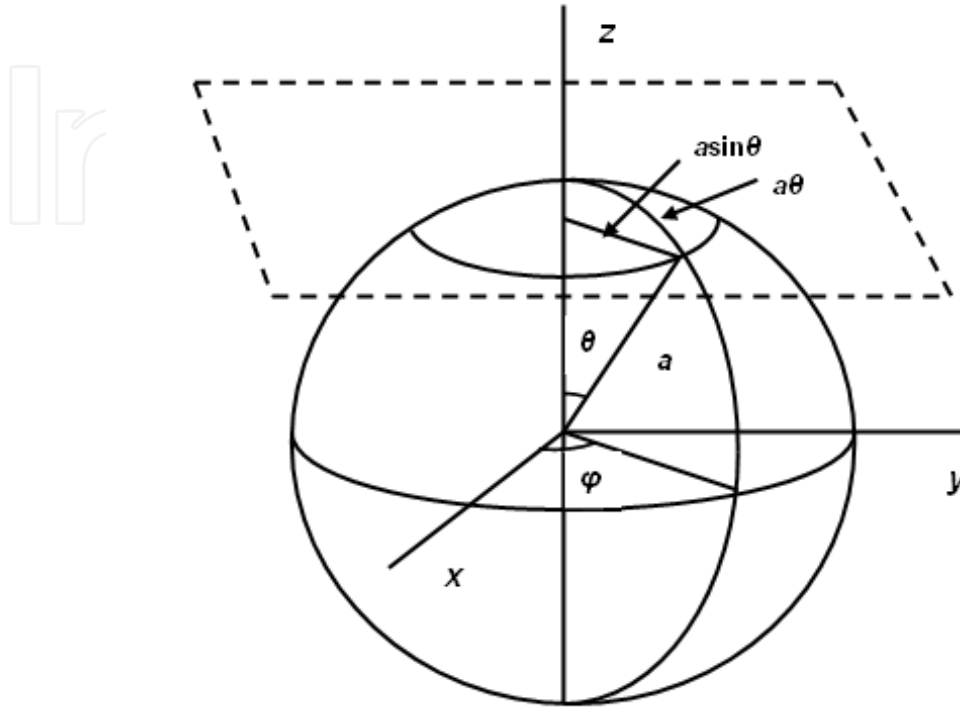


Figure C.1. Spherical surface with source at north pole ($\theta = 0$).

In order to compare the spherical surface solution with that of the flat surface solution (cf. Bhatnagar, et al., 2006), we notice that the corresponding circular wave-fronts on the flat surface will have radii of $a\theta$ and circumferences $2\pi a\theta$ (Fig. C.1). Thus the ratio of the intensities of the waves will be

$$\frac{I_{ModelC}}{I_{ModelB}} = \frac{I_{spherical}}{I_{flat}} = \frac{\theta}{\sin \theta} \quad (C.3)$$

Hence, the ratio of the amplitudes of the waves is

$$\frac{\psi_{ModelC}}{\psi_{ModelB}} = \frac{\psi_{spherical}}{\psi_{flat}} = \sqrt{\frac{\theta}{\sin \theta}} \quad (C.4)$$

Table C.1 shows the ratios of the wave intensities and amplitudes in the spherical and flat surface solutions. The values are independent of the radius of the sphere and are therefore applicable to all spherical surfaces. The departures of the spherical surface solutions from those of the flat surface solutions are slight for small values of θ . Even at the equator ($\theta = \pi/2$), the enhancements of the wave intensity and amplitude are merely 57% and 25% respectively. The enhancement becomes progressively greater until the south pole ($\theta = \pi$) is reached, where it becomes infinite.

θ , deg	θ , rad	$\sin\theta$	$\frac{\theta}{\sin\theta}$	$\sqrt{\frac{\theta}{\sin\theta}}$
0	0	0	1	1
15	.2618	.2588	1.0115	1.0057
30	.5236	.5000	1.0472	1.0233
45	.7854	.7071	1.1107	1.0539
60	1.0472	.8660	1.2092	1.0996
75	1.3090	.9659	1.3552	1.1641
90	1.5708	1.0000	1.5708	1.2533
105	1.8326	.9659	1.8972	1.3774
120	2.0944	.8660	2.4184	1.5551
135	2.3562	.7071	3.3322	1.8254
150	2.6180	.5000	5.2360	2.2882
165	2.8798	.2588	11.1267	3.3357
180	3.1426	0	∞	∞

Table C.1. Intensity and Amplitude Ratios in Spherical and Flat Surface Solutions.

D. Wave propagation from finite line source in two dimensions

Consider a finite line source of strength q and length $2c$ in the $x - y$ plane, whose end-points are located at $(-c, 0)$ and $(c, 0)$ (Fig. D.1). The velocity potential ψ can be expressed as

$$\psi = \phi(x, y)T(t) \quad (\text{D.1})$$

where $\phi(x, y)$ satisfies the two-dimensional Laplace's equation

$$\frac{\partial^2 \phi}{\partial x^2} + \frac{\partial^2 \phi}{\partial y^2} = 0 \quad (\text{D.2})$$

The potential due to a line source constitutes a well-known problem in electrostatics (cf. Abraham & Becker, 1950). The equi-potential lines on which $\phi(x, y)$ is constant are con-focal ellipses with their foci located at the end-points of the line source. The lines of force are con-focal hyperbolas perpendicular to the ellipses (cf. Morse & Feshbach, 1953). In the case of a tsunami from a linear subduction zone, the ellipses represent the wave-fronts, whereas the hyperbolas are the lines along which the enrrgy is transferred (Fig. D.1).

The amplitude of the wave can be obtained by a practical approach similar to that of Tan & Lyatskaya (2009). An approximate expression for the perimeter of an ellipse with semi-major axis a and semi-minor axis b is found in the literature (cf. Weisstein, 2003):

$$L \approx \pi \sqrt{2(a^2 + b^2)} \quad (\text{D.3})$$

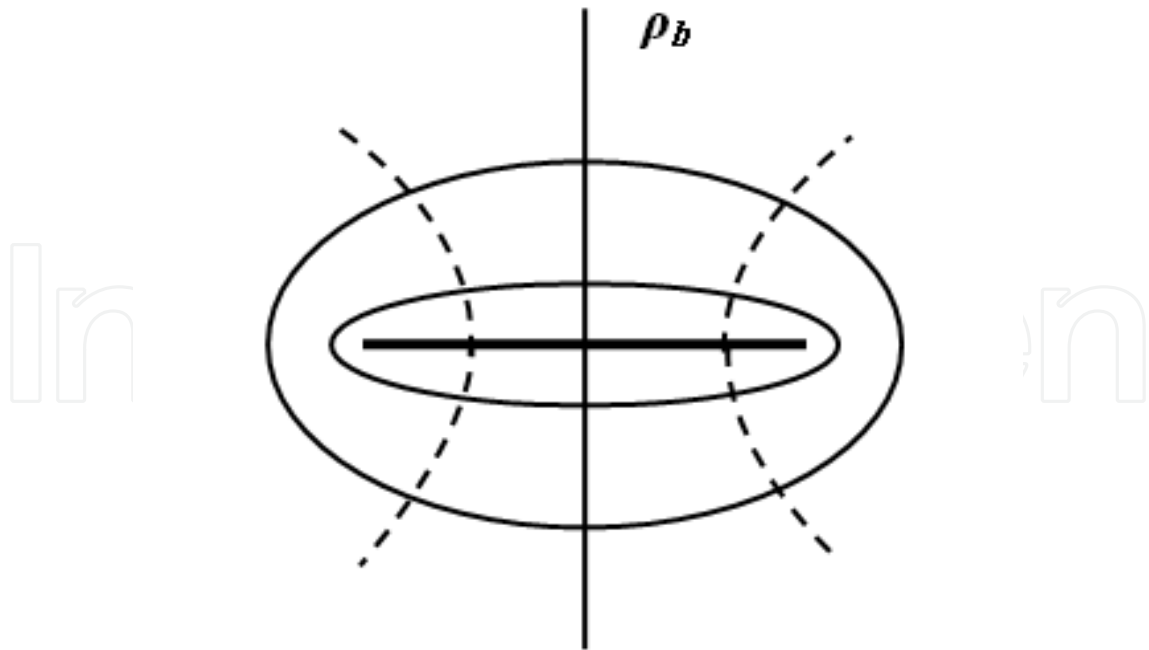


Figure D.1.Elliptical wave-fronts on which potential due to finite line source is constant.

From the property of the ellipse, $a^2 = b^2 + c^2$ (cf. Tan, 2008). Thus

$$L \approx \pi \sqrt{2b^2 + c^2} \tag{D.4}$$

As the elliptical wave-front propagates outwards, its intensity diminishes inversely as L , giving

$$I_{ModelD} \propto \frac{1}{\sqrt{b^2 + \frac{c^2}{2}}} \tag{D.5}$$

Hence, the wave amplitude varies as

$$\psi_{ModelD} \propto \frac{1}{\sqrt[4]{b^2 + \frac{c^2}{2}}} \tag{D.6}$$

Along the y -axis or the perpendicular bisector of the line source, we can equate b with the distance from the center of the source along that axis ρ_b :

$$\psi_{ModelD} \propto \frac{1}{\sqrt[4]{\rho_b^2 + \frac{c^2}{2}}} \tag{D.7}$$

One can compare the wave amplitude in Model D with that of a point source of equivalent strength (Model B). Remembering Eq. (B.18), we can re-write Eq. (D.7) as:

$$\psi_{ModelD} \propto \frac{1}{\sqrt{\rho_b}} \frac{1}{\sqrt[4]{1 + \frac{c^2}{2\rho_b^2}}} = \psi_{ModelB} \frac{1}{\sqrt[4]{1 + \frac{c^2}{2\rho_b^2}}} \quad (D.8)$$

Thus

$$\frac{\psi_{ModelD}}{\psi_{ModelB}} = \frac{1}{\sqrt[4]{1 + \frac{c^2}{2\rho_b^2}}} \quad (D.9)$$

Table D.1 shows the comparative values of the wave amplitudes in the line source (Model D) and point source (Model B) models. They differ greatly near the origin ($\rho_b = 0$), but the solutions begin to converge away from the origin. At $\rho_b = .2c$, the Model D value is only half that of Model B. For $\rho_b > c$, the difference is below 10%. For $\rho_b = 10c$, the two solutions are virtually indistinguishable.

$\frac{\rho_b}{c}$	$\frac{1}{\sqrt[4]{\rho_b^2 + \frac{c^2}{2}}}$	$\frac{1}{\sqrt{\rho_b}}$	$\frac{1}{\sqrt[4]{1 + \frac{c^2}{2\rho_b^2}}}$
0	1.189	∞	0
.1	1.183	3.162	.374
.2	1.167	2.236	.521
.3	1.141	1.826	.625
.4	1.109	1.581	.702
.5	1.075	1.414	.760
.6	1.038	1.291	.804
.7	1.003	1.195	.839
.8	.968	1.118	.866
.9	.935	1.054	.887
1.0	.904	1.000	.904
1.5	.777	.816	.951
2.0	.687	.707	.971
3.0	.570	.577	.987
4.0	.496	.500	.992
5.0	.445	.447	.995
6.0	.407	.408	.996
7.0	.377	.378	.997
8.0	.353	.354	.998
9.0	.333	.333	.999
10.0	.316	.316	1.000

Table D.2. Amplitude Ratios in Line Source and Point Source Solutions.

Author details

A. Tan, A.K. Chilvery and M. Dokhanian
Alabama A & M University, Normal, Alabama, USA

S.H. Crutcher
US Army RD&E Command, Redstone Arsenal, Alabama, USA

Acknowledgement

This study was partially supported by a grant from the National Science Foundation HBCU-UP HRD 0928904.

6. References

- Abraham, M. & Becker, R. (1950). *The Classical Theory of Electricity and Magnetism*, Blackie and Sons, ISBN 545854, London, UK.
- Bhatnagar, V.P., Tan, A. & Ramachandran, R. (2006). On response of the exospheric temperature to the auroral heating impulses during geomagnetic disturbances, *J. Atmos. Sol. Terr. Phys.*, Vol. 68, pp. 1237–1244, ISSN 1364-6826, UK.
- Boussinesq, J. (1871). Théorie de l'intumescence liquide appelée onde solitaire ou de translation se propageant dans un canal rectangulaire, *Comptes Rendus*, Vol. 72, pp. 755-759, ISSN: 0567-7718, France.
- Cecioni, C. & Bellotti, G. (2011). Generation and propagation of frequencydispersive tsunami, In *The tsunami threat – Research and technology* (2011). Mörner, N.-A., ed., InTech, ISBN 978-953-307-552-5, Croatia.
- Coulson, C.A. (1955). *Waves*, Oliver and Boyd, ISBN 0582449545, Edinburgh, UK.
- Dudley, W.C. & Lee, M. (1988). *Tsunami!*, University of Hawaii Press, ISBN: 0824819691, Honolulu, Hawaii, USA.
- Elmore, W.C. & Heald, M.A. (1969). *Physics of Waves*, Dover, ISBN 978-0486649269, New York, USA.
- Helene, O. & Yamashita, M.T. (2006). Understanding the tsunami with a simple model. *Eur. J. Phys.*, Vol. 27, pp. 855-863, ISSN 0 143-0807, UK.
- Herring, P.J. & Clarke, M.R. (1971). *Deep Oceans*, Praeger Publishers, ISBN-10: 0213176165, New York, USA.
- Hickey, M.P. in *The tsunami threat – Research and technology* (2011). Mörner, N.-A., ed., InTech, ISBN 978-953-307-552-5, Croatia.
- Imteaz, M.A., Imamura, F. & Naser, J, Numerical model for multi-layered tsunami waves, In *The tsunami threat – Research and technology* (2011). Mörner, N.-A., ed., InTech, ISBN 978-953-307-552-5, Croatia.
- Irving, J. & Mullineaux, N. (1959). *Mathematics in Physics and Engineering*, Dover, ISBN 9780123742506, New York, USA.
- Kanamori, H. (1977). The energy release of great earthquakes, *J. Geophys. Res.*, Vol. 82, pp. 2981-1987, ISSN: 2156-2202, USA.

- Kanamori, H. (2010). *Revisiting the 1960 Chilean earthquake*, in USGS Open-File Report 2010-1152, U.S. Geological Survey, USA.
- Karling, H.M. (2005). *Tsunamis*, Nova Science Publ. Inc., ISBN-10: 1594545189, Hauppauge, New York, USA.
- Korteweg, D.J. & de Vries, G. (1895). On the change of form of long waves advancing in a rectangular canal and on a new type of long stationary waves, *Phil. Mag.*, Ser. 5, Vol. 39, pp. 422-443, ISSN: 13642812, UK.
- Kowalik, Z., Knight, W., Logan, T., and Whitmore, P. (2005). Numerical modeling of the global tsunami: Indonesian tsunami of 26 December 2004, *Sci. Tsunami Hazards*, Vol. 23, pp. 40-56, ISSN 8755-6839, USA.
- Lamb, H. (1993). *Hydrodynamics*, Cambridge University Press, ISBN: 0521458684, Cambridge, UK.
- Lay, T., Kanamori, H., Ammon, C., Nettles, M., Ward, S., Aster, R., Beck, S., Brudzinski, M., Butler, R., DeShon, H., Ekström, G., Satake, S. & Sipkin, S. (2005). The great Sumatra-Andaman earthquake of 26 December 2004, *Science*, Vol. 308, pp. 1127-1133, ISSN: 0036-8075, USA.
- Margaritondo, G. (2005). Explaining the physics of tsunamis to undergraduate and non-physics students, *Eur. J. Phys.*, Vol. 26, pp. 401-407, ISSN 0 143-0807, UK.
- Mörner, N.-A. (2010). Natural, man-made and imagined disaster, *Disaster Advances*, 3(1), pp. 3-5, ISSN: 0974-262X, India.
- Morse, P.M. & Feshbach, H. (1953). *Methods of Theoretical Physics*, McGraw-Hill, ISBN 9780070433168, New York, USA.
- Pararas-Carayannis, G. (1976). *The Earthquake and Tsunami of 29 November 1975 in the Hawaiian Islands*, International Tsunami Information Center Report, USA.
- Parker, B.B. (2012). *The Power of the Sea: Tsunamis, Storm Surges, Rogue Waves, and Our Quest to Predict Disasters*, Palgrave MacMillan, ISBN-10: 0230120741, New York, USA.
- Rayleigh, Lord (1914). On the theory of long waves and bores, *Proc. Roy. Soc.*, Ser. A, Vol. 90, pp. 219-225, ISSN: 0950-1207, UK.
- Russell, S. (1844). Report on waves, *British Association Repots*, UK.
- Sharman, R.V. (1963). *Vibrations and Waves*, Butterworths, ISBN 9780408692007, London, UK.
- Smith, C.R. & Demopoulos, A.W.J. (2003). In *Ecosystems of the Deep Ocean*, Tyler, P.A. ed., Elsevier, ISBN-10:044482619X, Amsterdam, Holland.
- Stewart, G.B. (2005). *Catastrophe in Southern Asia: The Tsunami of 2004*, Lucent Books, ISBN-10: 1590188314, Farmington Hills, Michigan, USA.
- Stoker, J.J. (1957). *Water Waves*, Interscience, ISBN 9780471570349, New York, USA.
- Tan, A. (2008). *Theory of Orbital Motion*, World Scientific, ISBN 9789812709110, Singapore.
- Tan, A & Lyatskaya, I. (2009). Alternative tsunami models. *Eur. J. Phys.*, Vol. 30, pp. 157-162, ISSN 0 143-0807, UK.
- The Indian Ocean Tsunami: The Global Response to a Natural Disaster*, P.P. Karan & S.P. Subbiah ed. (2011), University Press of Kentucky, ISBN: 978-0-8131-2652-4, Lexington, Kentucky, USA.
- The tsunami threat – Research and technology* (2011). Mörner, N.-A., ed., InTech, ISBN 978-953-307-552-5, Croatia.

Towne, D.H. (1967). *Wave Phenomena*, Dover, ISBN 9780201075854, New York, USA.

Tsunami (2012). Lopez, G.I. ed., InTech, ISBN 979-953-307-835-8, Croatia.

Weisstein, E.W. (2003). *CRC Concise Encyclopedia of Mathematics*, Chapman-Hall, ISBN 1584883472, Champaign, USA.

Zatzkis, H. in *Fundamental Formulas in Physics* Vol. 1 (1960). Menzel, D.H., ed., Dover, ISBN 9780486605951, New York, USA.

IntechOpen

IntechOpen